NASA/TM—1999-209195

Neural-Net Processing of Characteristic Patterns From Electronic Holograms of Vibrating Blades

Arthur J. Decker
Glenn Research Center, Cleveland, Ohio

National Aeronautics and
Space Administration

Glenn Research Center

June 1999

Available from

NASA Center for Aerospace Information
7121 Standard Drive
Hanover, MD 21076
Price Code: A03

National Technical Information Service
5285 Port Royal Road
Springfield, VA 22100
Price Code: A03

NEURAL-NET PROCESSING OF CHARACTERISTIC PATTERNS

Arthur J. Decker
NASA Glenn Research Center
Cleveland, Ohio 44135

Abstract: Finite-element-model-trained artificial neural networks can be used to process efficiently the characteristic patterns or mode shapes from electronic holograms of vibrating blades. The models used for routine design may not yet be sufficiently accurate for this application. This document discusses the creation of characteristic patterns; compares model generated and experimental characteristic patterns; and discusses the neural networks that transform the characteristic patterns into strain or damage information. The current potential to adapt electronic holography to spin rigs, wind tunnels and engines provides an incentive to have accurate finite element models for training neural networks.

Introduction

Efficient, automated, goal-directed interpretation of visualization patterns is an on-going challenge. These patterns are easily generated with a multitude of photonic and non-photonic methods. The photonic methods include, for example, interferometry, holography, moire, fluorescence spectroscopy, speckle photography and interferometry, photometry, radiometry, x-ray and visible-light shadowgraphy, schlieren, and other forms of deflectometry, Mie and Rayleigh scattering, and particle imaging methods. These patterns are now days easy to record and easy to digitize for computer processing. However, processing the patterns for automation or robotics applications is not straightforward. The classical approach to processing was to dissect the patterns and convert them into distributions of properties, including density, strain, displacement, velocity, refractive-index, polarization, or temperature fields. These distributions are often extremely complex. Their two- and three-dimensional visualizations are often no easier to use than the original visualization patterns. The information important for automation is often buried subtly in the entire pattern. For example, strain or displacement fields are not necessarily informative to a machine intended to monitor for structural damage. The effects of damage on the pattern may be small or distributed over the entire pattern. Artificial neural-net technology offers a solution of the interpretation problem. Artificial neural networks can be trained by example to inspect a pattern for a particular event, state, or property. The examples can be generated experimentally or with computational models and can contain exactly the outputs required by the machine. This chapter discusses a particular example of this process for a visualization pattern from electronic holography, electronic-speckle-pattern interferometry.

Artificial neural networks have been used to compare measured vibration-mode shapes with computed vibration-mode shapes (Decker, et. al., 1998a, 1998b). The mode shapes were displayed using electronic holography, also known as television holography or electronic speckle pattern interferometry (ESPI). Mode shapes were also computed using a finite element model together with an electronic holography model. The neural networks were then trained with model-generated or measured training sets. The model-trained nets were used to inspect measured mode shapes, and vice versa.

The neural networks can be trained to flag differences between a finite element model and a structure, typically a fan blade, where the mode-shape differences are caused by run-induced damage or by manufacturing defects. Unfortunately, the mode-shape differences can also result from an inadequate finite element model.

Workstation or PC-resident artificial neural networks offer significant advantages for inspection, if they can be trained adequately. Inspections of mode shapes have been conducted in real time at 30 frames per second. The neural networks can be trained to ignore noise. For example, neural networks have been trained to handle the laser speckle effect. The speckle effect is evident in

the characteristic patterns of electronic time-average holography (fig. 1). The characteristic patterns, in turn, display the vibration-mode shapes. Another advantage is that neural networks can be trained to detect structural changes or damage from an entire pattern rather than a point measurement. In effect, the entire structure serves as a damage gauge.

Currently, a technique such as television holography offers an excellent chance to exploit developments in fiber optics and miniaturized imaging technology. Figure 2 compares characteristic patterns of a vibration mode recorded directly and also through a 20-ft (6 m) fiberscope. The fiberscope can be used to collect characteristic patterns remotely from engine components such as a fan. Videoscopes offer a similar capability. But characteristic patterns are not especially sensitive to structural changes such as crack formation. Methods for rapid, efficient inspection and interpretation of the patterns are required; artificial neural networks are indeed fast, efficient and sensitive.

Neural networks are well suited, in principle, for implementing optical inspections using electronic holography, but the user must accommodate some real limitations as well. Feedforward neural networks may train very slowly, although slow learning has never been a problem with the noisy characteristic patterns of electronic holography. A more serious limitation is that neural networks are in effect hard-to-define, hard-to-quantify black boxes. It is hard to predict a priori the response of a net to a pattern differing even slightly from the patterns of the training set. A feedforward network with one hidden layer is thought to serve as an example (Ripley, 1996) of a non-parametric fitting method called projection pursuit regression. Predictably, neural nets have the same weaknesses as other models developed from exemplars, measurements, or training sets. Over-fitting is always a hazard. Over-fitting effectively can be used to make a neural net sensitive to small changes in mode shape. But an over-fitted neural network will not learn to handle irrelevancies such as the laser speckle effect. Ordinary statistical practice has some nice computational machinery for designing experiments and producing good fits to the measurements. Similar techniques for neural networks don't work as well. The performance of a feedforward neural network is not a sensitive function of the number of hidden layer nodes or the number of training set examples. Hence, optimization can be a tedious process. A straightforward design-of-experiments, response-surface study has been used to optimize feedforward networks for handling speckled characteristic patterns (Decker, et. al., 1997).

Creating adequate training sets remains the major challenge to exploiting optical and neural-net technologies for inspecting the characteristic patterns of vibrating structures. Training sets are created most efficiently and most affordably from a computational model such as a finite element model. A hybrid would be the next best approach, where a computational model was adapted with some experimental data. The least affordable and least efficient approach is to train the neural network with the mode shapes from actual structures.

So far, the finite element models used for designing fan blades have been inadequate for generating training sets for generally curved blades. Feedforward and adaptive resonance theory (ART) neural networks easily recognize that measured and model generated mode shapes are different. This discrepancy is especially a problem, when training neural networks to distinguish damaged from undamaged blades. Damage such as a crack affects the mode shapes encoded in the characteristic patterns less than the modeling discrepancies affect the mode shapes.

One might ask whether it is important to have exacting critics of simulation-generated visualization patterns such as the characteristic patterns of electronic holography. Of course, the scientific method presumes that good models and theories will predict the measurements actually made as well as they can be made. But a less-than-perfect model might be quite adequate in a design procedure, and the difference flagged by a neural network might be deemed quite irrelevant. Then the challenge is to train the neural network to ignore the "irrelevancies". So far, we have accomplished that goal for the laser speckle effect, a real physical phenomenon that is of no interest to the blade designer. Variations of the mode shapes caused by damage and by manufacturing defects probably are interesting to blade designers and manufacturers, however.

We outline briefly, in any case, the effectiveness of finite-element-model-trained neural networks for inspecting mode shapes encoded in the characteristic fringe patterns from electronic holography. The technology for acquiring these patterns in test facilities and jet engines has

improved greatly in this decade, and the computer technology to process the patterns has clearly improved.

Electronic Holography

In the history of laser applications, time-average holography is an ancient method for visualizing mode shapes (Powell and Stetson, 1965). A hologram is recorded of an object vibrating in an eigenmode. Off-axis-reference-beam holograms were recorded, originally, so as to separate the self-interference, real and virtual image waves during reconstruction. The intensity of the virtual-image wave was observed modulated with a term proportional to the square of

$$J_0(2\pi K \bullet \delta) \tag{1}$$

where J_0 is the zero-order Bessel function of the first kind, K is the sensitivity vector, and δ is the displacement-amplitude vector measured in units of the wavelength of light. The displacement amplitude δ varies from point to point on the vibrating object, and vanishes on the nodes of vibration. The Bessel function has its maximum value for zero argument; hence the pattern is brightest on a node. Consequently, time-average holography provides spectacular visualizations of mode shapes. Silver-halide-emulsion holograms, however, are time-consuming to record. Automated inspection of the so-called Bessel fringe patterns is difficult to accomplish.

Electronic or television holography (Stetson and Brohinsky, 1988) is both fast and potentially quantitative for vibration analysis. The low resolution of the CCD array used to record the holograms is the major penalty. A couple of tricks are used to handle this penalty and the effects of the interferences between the reconstructed waves. First, a focused image hologram is recorded. That is, a lens forms an image of the vibrating object on the CCD array, and that image is combined with a reference beam. The reference beam is coaxial, or almost coaxial, with the object beam. This combination of beams is accomplished with a beam splitter. The interference pattern on the CCD array, formed between the object and reference beams, is a true hologram. The virtual and real-image terms of the hologram overlap exactly on the recording medium (the CCD array). The hologram is given by

$$I_R(x, y) + I_O(x, y) + 2\sqrt{I_R(x, y)}\sqrt{I_O(x, y)}\cos[\theta(x, y)]J_0(2\pi K \bullet \delta) \tag{2}$$

where $I_R(x, y)$ is the reference beam intensity, $I_O(x, y)$ is the object beam intensity, and $\theta(x, y)$ is the object-to-reference phase. The argument of the Bessel function is defined above.

The third term, which encodes the real-image and virtual-image waves in silver-halide holography, contains the useful "characteristic" pattern or mode shape of the vibrating object. Both θ and I_O are random variables. Their randomness is responsible for the laser speckle effect.

The first two terms, the self-interference terms, can be eliminated by using two holograms. The holograms can be recorded in two adjacent frames or two adjacent fields of the CCD camera. The speckle patterns of the two holograms must be correlated. The speckle size must be larger than the separation between adjacent television lines, if two fields are used. The object-to-reference phase θ is shifted by π between the two holograms, and the holograms are subtracted. The difference is given by

$$4\sqrt{I_R(x, y)}\sqrt{I_O(x, y)}\cos[\theta(x, y)]J_0(2\pi K \bullet \delta) \tag{3}$$

The square or absolute value of this quantity can be displayed as in fig. 1. The use of adjacent fields allows two short-exposure, time-average holograms to be recorded (frame straddling). This arrangement is more immune to environmental disturbances or rigid-body motion.

Phase shifting and frequency shifting can be combined in additional frames or fields to extract the argument of the Bessel function, but only two frames or fields, used to derive the characteristic pattern of expression (3), are necessary for the neural-network application that we discuss.

Comparison of Calculated and Measured Bessel Fringe Patterns

Expression (3) is easy, in principle, to model. Consider fan blades, for example. Figures 1 and 2 show characteristic patterns of fan blades. The three components of the displacement amplitude δ are computed at each point of the visible surface of the blade using a finite element model (Schaeffer, 1979). MSC/NASTRAN Solution 103 has been used for the examples in this chapter, and is used routinely to design blades. The sensitivity vector K is the difference between the unit vector of the incident light ray at a point on the blade and the unit vector of the reflected principal light ray at that point. The principal light ray from a point on the blade is the light ray passing through the center of the entrance pupil of the imaging lens. The sensitivity vector depends somewhat on the profile of the blade. This dependence is often negligible, and the projected image of the profile can be used to evaluate the sensitivity vector.

Both I_O and θ are random variables. One value of each is assigned to a speckle. The minimum size of a speckle will be the pixel size of the CCD camera. The imaging optics can produce larger speckles. For comparison with finite element models, a single speckle may be sampled for each node in the finite element grid. The characteristic pattern is displayed then with the coarse resolution of the finite element grid. In all cases, a suitable model is to select I_O from a negative exponential distribution and to choose θ uniformly distributed from 0 to 2π. Neural networks trained with model-generated speckle and experimental speckle perform equally well. The same cannot be said, in general, when comparing finite-element and experimental displacement distributions. But the performance is good for a cantilever plate, when either model-generated or experimental characteristic patterns are presented to a finite-element-model-trained neural network.

Figure 3 shows characteristic patterns for the first chord-wise mode. Figure 3a was reconstructed from an old silver halide hologram of a vibrating blade. Figures 3b, 3c and 3d show the first chord-wise mode for a cantilever plate (Decker, et. al., 1998a). Figure 3b was generated from electronic holograms recorded from adjacent frames (30 frames per second) with a RS-170 CCD camera with the standard 480 vertical X 640 horizontal pixels. Figure 3c is a finite-element resolution characteristic pattern calculated using expression (3) and a finite-element model of the plate. Figure 3d was an experimental characteristic pattern as in fig. 3b, but sampled at the finite-element resolution used to create fig. 3c. The plate for figs. 3b, 3c and 3d was 7.62 cm (3 in) wide by 15.24 cm (6 in) long with a thickness of 0.254 cm (0.1 in). The material was 6061-T6 Aluminum with a Young's Modulus of 66.19 GPa (9.6×10^6 psi), a Poisson's ratio of 0.33 and a Mass Density of 2712.832 kg/m^3 (2.536×10^{-4} lbs sec^2/in^4). The finite element model consisted of a 20x42 mesh of quadrilateral elements along the mid-thickness of the plate. The bottom edge was constrained in all six degrees of freedom.

The characteristic patterns in figs. 3c and 3d resemble one another sufficiently that a neural network trained with the model-generated patterns as in fig. 3c responds correctly to experimental patterns as in fig. 3d. Furthermore, a simple finite-element model, which includes cracks, was sufficient to train a neural network to recognize damage located 3.81 cm (1.5 in) from the long edge and 2.54 cm (1 in) from the bottom edge. The model-trained feedforward neural-net discussed in the next section correctly distinguished cracked from undamaged vibrating cantilevers at about 30 frames per second. The neural net monitored the entire characteristic pattern, thereby effectively making the entire plate a damage gage. Unfortunately, this success was not repeated for a twisted blade.

Figure 4 (Decker, et. al., 1998b) shows a mounted twisted blade that was used to test model-trained and experimentally trained neural networks for processing twisted-blade characteristic patterns. Three blades were manufactured. The blade geometry is of constant cross-section and has a twist that varies linearly from 0 degrees at the root to 30 degrees at the tip. Blade dimensions are chord, 8.72 cm (3.433 in); maximum thickness to chord ratio, 0.037; and span, 15.24 cm (6.0 in). The blade material was the same aluminum used to manufacture the cantilevers. The mount was inserted in a vice and held with the same force for all tests. One blade was cracked by high cycle fatigue in the first mode at about 199 Hz. Figure 5 shows the characteristic pattern of the first mode and an insert region. The fatigue-induced crack (not visible) is at the bottom and right edge of the insert region in one of the three blades. The crack itself does not cause a visible change in the full-scale characteristic patterns, and the neural networks could not be trained to recognize damage from the

full-scale characteristic patterns. By contrast, the neural networks, in the case of the cantilever, could be trained to recognize damage from the full-scale characteristic patterns. But the damage in the cantilever was located 2.54 cm (1 in.) from the bottom edge; whereas the crack in the twisted blade was located right at the bottom edge.

Figure 6 shows zoomed characteristic patterns in the insert region of fig. 5 for undamaged and cracked blades. Here, the characteristic patterns of the undamaged and cracked blades clearly differ in the right half. Neural networks have been trained successfully by experimental example to flag this kind of damage. The same cannot be said of the finite element model. A finite element model was constructed with a 20x42 mesh of quadrilateral elements along the mid-thickness of the airfoil. A crack at the root, extending from 87% to 100% of chord, was modeled by releasing all six degrees of freedom at the root.

The model-generated characteristic patterns of the blade differ noticeably from the measured characteristic patterns. Figure 7 shows a model-calculated first mode. This simulation was computed at high vibration amplitude and brightened to define the node line better. The node line extending upward to the left intersects the left edge of the blade at different locations in the model-generated and measured patterns as can be seen by comparing figs. 5 and 7. The difference between model-generated and measured modes is especially noticeable in the insert region. Figure 8 shows a model-calculated characteristic pattern in that region for an undamaged blade. The model-calculated pattern does not resemble the measured pattern shown in fig. 6. Changing the mesh size does not affect the results.

The cantilever example demonstrated that finite-element-trained neural networks are effective for damage detection, but the twisted-blade example demonstrated that at least one design-grade finite element model is not adequate for real twisted blades. Given adequate models, there are some simple rules for constructing, training and using artificial neural networks for inspecting mode shapes.

Neural Networks for Inspecting Mode Shapes

The terminology "artificial neural network" refers to a rather large number of computational algorithms that implement or emulate the parallel processing of data (Rumelhart, et. al., 1986). Some of the algorithms derive from non-parametric statistical analysis, model building, etc. (Ripley, 1996). "Neural network" refers to the superficial similarity of some architectures such as the feedforward and adaptive resonance theory (ART) nets to biological neural networks. The artificial neural networks that we use to process characteristic patterns are generated or constructed or trained from training sets of exemplars. The exemplars consist of finite-element-resolution characteristic patterns and associated output patterns or flags. A properly trained neural network will respond with the correct output pattern or flag when presented with an input characteristic pattern.

The neural networks that we use to process characteristic patterns can be divided roughly into two classes. The classes correspond to two training or learning generalities called "unsupervised learning" and "supervised learning". Unsupervised learning is essentially automatic classification. For example, an algorithm that learns to divide a training set into two classes consisting of undamaged-blade characteristic patterns and cracked-blade characteristic patterns, without explicit a priori specification of the damage property, is accomplishing unsupervised learning.

In supervised learning, the neural net is trained to associate each characteristic pattern with a specific output. For example, the output could be the finite-element-model-generated strain or strain-energy pattern. A better choice follows from noting that the characteristic patterns such as represented by expressions (1) and (3) encode the sensitivity-vector-projected components of the displacement vectors. Hence, the sensitivity-vector-projected displacement vector and its derivatives are more appropriate outputs for the neural networks. Also the second derivatives of the displacement are related to the bending induced strain for a thin plate or blade (Vest, 1979). For example, for a cantilevered thin plate such as the plate yielding the characteristic patterns in fig. 3, the bending induced strain along the x axis is proportional to

$$\partial^2\delta_z/\partial x^2 + \nu\,\partial^2\delta_z/\partial y^2 \qquad (4)$$

where ν is Poisson's Ratio. The component δ_z is perpendicular to the cantilever plate and is the only significant component for a cantilever vibrating at the small amplitudes excited for electronic holography. The sensitivity vector K tends to be perpendicular to a blade surface for sensible applications of electronic holography; hence $K \bullet \delta$, and its second derivatives, can substitute approximately for δ_z and its second derivatives, in many cases. Another reason for using the second derivatives of $K \bullet \delta$ is that the second derivatives computed from double-exposure holograms have proven to be quite sensitive to cracking and damage (Decker, 1990). Figure 9 shows the contour plots of the outputs of a feedforward neural network that was model trained with undamaged and cracked-blade characteristic patterns of the cantilever of fig. 3. The actual mode that was used for the test is also shown. The outputs, which were displayed at 30 frames per second by a workstation, show the second chord-wise derivatives $\partial^2(K \bullet \delta)/\partial y^2$ of the finite-element-model-calculated displacement fields of the undamaged and cracked cantilevers.

The best example of a neural network subject to supervised training, as well as the net used most often by the author for inspecting characteristic patterns of vibrating blades, is the feedforward network. That neural network (fig. 10) is represented by interconnected processing nodes (neurons) connected with weighted connections (synapses). The nodes are arranged in layers. Signals are passed forward from nodes in layers on the left to nodes in layers on the right; hence, the net is called a feedforward artificial neural network. Normally, a layer is connected forward only with the layer on the right and receives signals only from nodes on the left. Sometimes, the input layer is also connected to the output layer. The nodes in the input layer typically represent connections for application of the input data and do no processing. For example, a characteristic pattern having a resolution equal to the number of values of $K \bullet \delta$ from the finite element mesh of 20x42 elements has 21x43 pixels. Hence, the neural network requires 903 input nodes or connections. The next layer to the right is called a hidden layer. Each node in this first hidden layer receives inputs from all the input nodes. Each input value, including a unit bias, is multiplied by a weight; the weighted inputs are summed; the sum is transformed by a non-linear function, usually a logistic (sigmoid) function; and the result of the transformation constitutes the output of the node. The outputs of the hidden-layer nodes may be sent to another hidden layer or to an output layer, whose outputs are accessible. The output nodes may function exactly like the hidden-layer nodes, or may simply form a linear sum of their weighted inputs. As an example, the chord-wise numerical second derivative of $K \bullet \delta$ can be estimated at each point from the values of $K \bullet \delta$ at the point and the adjacent points in the same row. There will be 19x43 values of the second derivative and 817 output nodes. The training set for this neural network will then contain records of 903 inputs and 817 outputs.

Determining the optimum numbers of nodes in a hidden layer, of hidden layers, and of training records is not straightforward. In general, any function mapping the 903 inputs into the 817 outputs can be implemented with a neural network with one hidden layer and an output layer. The hidden layer and output layer use logistic (sigmoid) transfer functions or unit step function. The outputs must be normalized somewhere in the range form 0 to 1 (typically 0.2 to 0.8) to accommodate the transfer functions.

A study has been performed to determine the optimum numbers of hidden-layer nodes and training records in a single-hidden-layer neural network for processing characteristic patterns of vibrating blades (Decker, et. al., 1997). The study involved model generated characteristic patterns, but employed design-of-experiments (DOE) and response-surface-methods (RSM) for optimization, as if the patterns had been recorded experimentally. A major objective of the study was to train feedforward nets to respond correctly to characteristic patterns having arbitrary speckle patterns. The results of that study can be presented as two simple rules:

(1) The training set should contain uncorrelated speckle patterns for each Bessel fringe pattern equal in number to 10% of the number of pixels in a pattern.

(2) The number of hidden-layer nodes should equal about 3 nodes for each Bessel fringe pattern.

Hence, a neural net, which is intended to distinguish cracked from undamaged blades at a single amplitude of vibration using 1000-pixel characteristic patterns, will have 200 records in the training set and about 6 hidden-layer nodes. These rules did not seem to be very sensitive to optical effects such as pixel saturation. The rules are specific to speckled fringe patterns and are not necessarily applicable to other applications of neural networks.

Once the feedforward architecture and training set have been selected, the neural net must be trained. A detailed discussion of the training algorithms and their mathematical representations is beyond the scope of this chapter and frankly adds nothing to the NDE applications. Software packages are available commercially for constructing nets and training them. Training is discussed extensively in the literature. Briefly stated, training consists of minimizing an energy function consisting of the sum of mean-square-errors between the net-generated outputs and the training-set outputs, or some variation. The energy is expressed in weight space and is to be minimized by adjusting the weights. The weights are modified in the process of performing a steepest decent search called back propagation. A number of variations of the basic algorithm, as well as feedforward architectures, exist.

Feedforward neural nets, intended to distinguish cracked from undamaged blades, train very quickly, if there is a significant difference between the characteristic patterns of the cracked and undamaged blades. Training occurs in a few minutes on a workstation. The whole-blade characteristic patterns, as in fig. 3, were used successfully to train a neural net to distinguish cracked from undamaged cantilevers. By contrast, a neural net could not be trained to distinguish cracked from undamaged twisted blades using experimental whole-blade patterns as in fig. 5. Either the net was over trained (too many hidden-layer nodes were used), thereby memorizing the speckle patterns, or the net didn't train at all. A net was trained successfully, however, using zoomed experimental characteristic patterns from the insert region in fig. 5. The zoomed patterns are shown in fig. 6.

The dot product $K \bullet \delta$ must be large enough in the zoomed region for training to succeed. An isolated blade can be oriented to accomplish this goal. The root region of a fan-mounted or blisk-mounted blade, the blade surface being nearly axial near the root, may be difficult to access adequately. Then fiberscopes, such as used to record fig. 2, must be inserted for a more favorable view.

Some of the results for the feedforward neural network have been checked using another neural-net architecture called Fuzzy ARTMAP. Adaptive Resonance Theory, ART, (Carpenter and Grossberg, 1987) has been used to refer to a number of neural-net architectures of which Fuzzy ARTMAP is one. Adaptive Resonance Theory Nets can be used to classify characteristic patterns using unsupervised or supervised learning. Fuzzy ARTMAP uses analog inputs and supervised formation of classes. The net trains very rapidly, but is not as compact in software as the feedforward net. In particular, the input vectors are effectively doubled in size; since both the input vector and its complement are presented to the net.

The most interesting result using Fuzzy ARTMAP is that the criterion, rule (1) above, for selecting the training-set size remains valid. Recall that rule (1) was developed using feedforward nets. A discussion of ART nets is beyond the scope of this chapter, but the training and functioning of ART nets appears to be quite different from feedforward nets trained by back propagation. Hence, the applicability of rule (1) is not obvious.

Concluding Remarks

The current potential to adapt electronic holography to non-destructive evaluation in facilities such as spin rigs and wind tunnels, or even to engines, calls for efficient processing of the characteristic patterns or mode shapes generated from electronic holograms. Artificial neural networks have been used to transform at nearly 30 frames per second the characteristic patterns or mode shapes of vibrating blades into damage information. The neural networks require training sets of exemplars, which are generated most efficiently from finite element models. Hence, there are new incentives to improve and couple the modeling, design and inspection processes.

References

Carpenter, G. A. and Grossberg, S. (1987) ART 2: stable self-organization of stable category recognition codes for analog input patterns. *Applied Optics* 26, 4919-4930.

Decker, A. J. (1990) Holographic interferometry with an injection seeded Nd:YAG laser and two reference beams. *Applied Optics* 29, 2696-2700.

Decker, A. J., Fite, E. B., Mehmed, O. and Thorp, S. A. (1997) Processing speckle patterns with model trained neural networks. In *Optical Technology in Fluid, Thermal, and Combustion Flow III, Proceedings of SPIE* 3172, eds S. S. Cha, J. D. Trolinger, and M. Kawahashi, 285-293.

Decker, A. J., Fite, E. B., Mehmed, O. and Thorp, S. A. (1998a) Vibrational analysis of engine components using neural-net processing and electronic holography. In *Advanced Non-Intrusive Instrumentation for Propulsion Engines, AGARD Conference Proceedings 598*, 33-1—33-6.

Decker, A. J., Fite, E. B., Thorp, S. A. and Mehmed, O. (1998b) Comparison of computational-model and experimental-example trained neural networks for processing speckled fringe patterns. In *International Conference on Optical Technology and Image Processing in Fluid, Thermal, and Combustion Flow, Proceedings of VSJ-SPIE '98,* on compact disc in pdf, paper AB002.

Powell, R. L. and Stetson, K. A. (1965) Interferometric vibration analysis by wavefront reconstruction. *Journal of the Optical Society of America* 55, 1593-1598.

Ripley, B. D. (1996) *Pattern Recognition and Neural Networks.* Cambridge: Cambridge University Press.

Rumelhart, D. E. and McClelland, J. L. (eds) (1986) *Parallel Distributed Processing: Explorations in the Microstructure of Cognition. Volume 1: Foundations.* Cambridge, MA: The MIT Press.

Schaeffer, S. G. (1979) *MSC/NASTRAN Primer Static and Normal Modes Analysis.* Mesa, CA: PDA Engineering.

Stetson, K. A. and Brohinsky, W. R. (1988) Fringe-shifting technique for numerical analysis of time-average holograms of vibrating objects. *Journal of the Optical Society of America* A5, 1472-1476.

Vest, C. M. (1979) *Holographic Interferometry.* New York: John Wiley & Sons, 146-177.

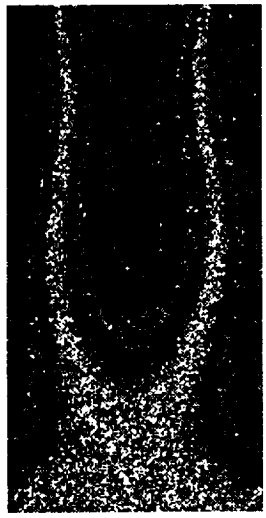

Figure 1: Speckled characteristic pattern from two electronic holograms of a vibrating cantilever. Cantilever is vibrating in its first chord-wise mode.

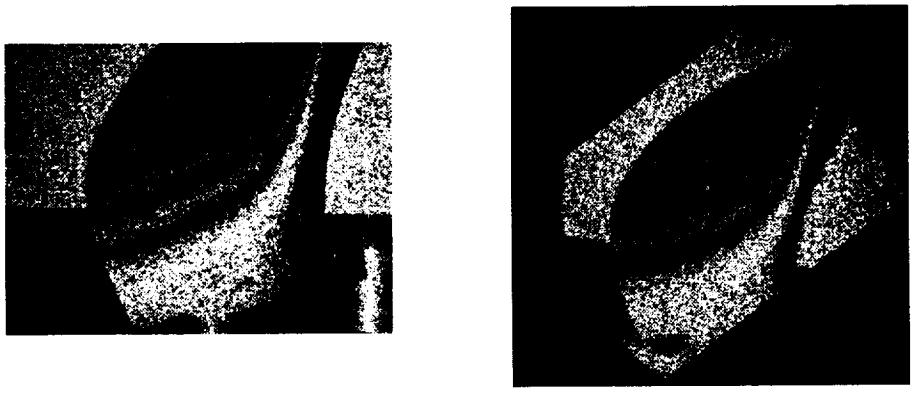

(a) (b)

Figure 2: Characteristic patterns generated from electronic holograms recorded (a) directly and (b) through a 20 ft fiberscope.

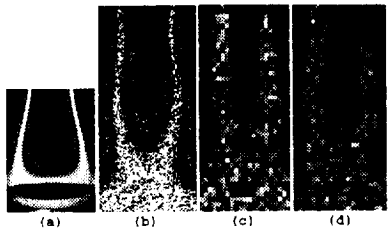

Figure 3: First chord-wise modes from: (a) silver halide hologram; (b) electronic holograms; (c) finite-element-resolution model of a cantilever plate; (d) electronic holograms sampled at finite element resolution.

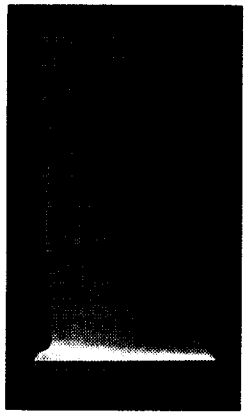

Figure 4: Model of twisted blade used to test finite-element-model-trained and experimentally trained neural networks for processing twisted-blade characteristic patterns.

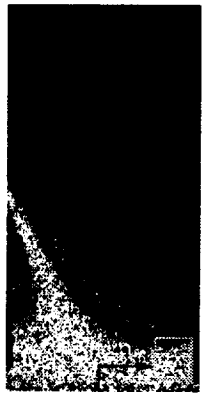

INSERT

Figure 5: Characteristic pattern of first mode of twisted blades. High-cycle fatigue cracking occurs in this mode in INSERT near its bottom right edge.

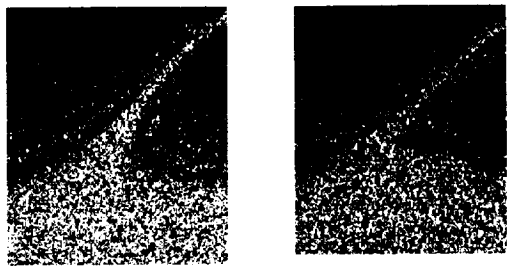

(a) (b)

Figure 6: Characteristic patterns in INSERT region for (a) undamaged and (b) cracked twisted blades.

Figure 7: First mode of twisted blade computed from finite-element model. Predicted node line extends further up left edge than experimental node line in Figure 5.

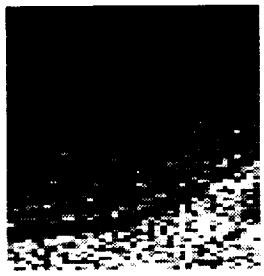

Figure 8: Finite-element-model-calculated characteristic pattern in INSERT region of Figure 5.

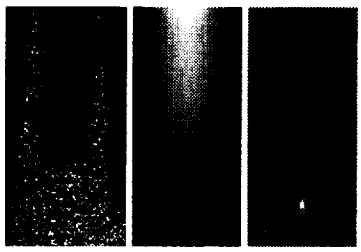

(a) (b) (c)

Figure 9: Performance of feedforward neural network trained with characteristic-pattern inputs and chord-wise second-derivative outputs. (a) is a representative characteristic pattern; (b) is the output for an undamaged cantilever; and (c) is the output for a cracked cantilever.

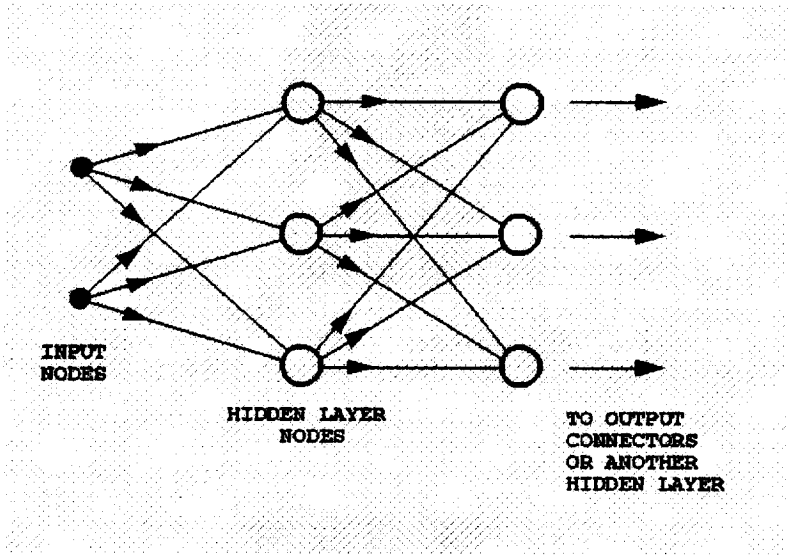

Figure 10: Feedforward artificial neural network. Bias inputs are not shown explicitly. Number of nodes in a layer and number of layers are arbitrary.

REPORT DOCUMENTATION PAGE

Form Approved
OMB No. 0704-0188

1. AGENCY USE ONLY (*Leave blank*)	2. REPORT DATE	3. REPORT TYPE AND DATES COVERED
	June 1999	Technical Memorandum

4. TITLE AND SUBTITLE

Neural-Net Processing of Characteristic Patterns From Electronic Holograms of Vibrating Blades

5. FUNDING NUMBERS

WU-323-78-00-00

6. AUTHOR(S)

Arthur J. Decker

7. PERFORMING ORGANIZATION NAME(S) AND ADDRESS(ES)

National Aeronautics and Space Administration
John H. Glenn Research Center at Lewis Field
Cleveland, Ohio 44135-3191

8. PERFORMING ORGANIZATION REPORT NUMBER

E-11710

9. SPONSORING/MONITORING AGENCY NAME(S) AND ADDRESS(ES)

National Aeronautics and Space Administration
Washington, DC 20546-0001

10. SPONSORING/MONITORING AGENCY REPORT NUMBER

NASA TM—1999-209195

11. SUPPLEMENTARY NOTES

Responsible person, Arthur J. Decker, organization code 5520, (216) 433-3639.

12a. DISTRIBUTION/AVAILABILITY STATEMENT

Unclassified - Unlimited
Subject Category: 29 Distribution: Nonstandard

This publication is available from the NASA Center for AeroSpace Information, (301) 621-0390.

12b. DISTRIBUTION CODE

13. ABSTRACT ***(Maximum 200 words)***

Finite-element-model-trained artificial neural networks can be used to process efficiently the characteristic patterns or mode shapes from electronic holograms of vibrating blades. The models used for routine design may not yet be sufficiently accurate for this application. This document discusses the creation of characteristic patterns; compares model generated and experimental characteristic patterns; and discusses the neural networks that transform the characteristic patterns into strain or damage information. The current potential to adapt electronic holography to spin rigs, wind tunnels and engines provides an incentive to have accurate finite element models for training neural networks.

14. SUBJECT TERMS

Neural nets; Holography; Nondestructive tests; Vibration mode; NASTRAN; Speckle holography; Fiber optics

15. NUMBER OF PAGES

18

16. PRICE CODE

A03

17. SECURITY CLASSIFICATION OF REPORT	18. SECURITY CLASSIFICATION OF THIS PAGE	19. SECURITY CLASSIFICATION OF ABSTRACT	20. LIMITATION OF ABSTRACT
Unclassified	Unclassified	Unclassified	